Nanoscale

PAPER

View Article Online
View Journal | View Issue

Published on 25 January 2018. Downloaded by Columbia University Libraries on 4/28/2019 8:51:51 PM.

Check for updates

Cite this: *Nanoscale*, 2018, **10**, 3307

Scalable production of core–shell nanoparticles by flash nanocomplexation to enhance mucosal transport for oral delivery of insulin†

Zhiyu He, [a,b,c,e,f] Zhijia Liu,[a,b] Houkuan Tian,[a,b] Yizong Hu,[f,g] Lixin Liu,[a] Kam W. Leong, [*a,b,c,d] Hai-Quan Mao*[a,b,e,f,g,h] and Yongming Chen*[a,b]

Scalable manufacturing continues to present a major barrier for clinical translation of nanotherapeutics. Methods available for fabricating protein-encapsulating nanoparticles in a scalable fashion are scarce. Protein delivery often requires multiple functionalities to be incorporated into the same vehicle. Specifically for nanoparticle-mediated oral delivery of protein therapeutics, protection in GI tract, site-specific release, facilitating transmucosal permeation, and enhancing epithelial transport are a few desirable features to be engineered into a nanoparticle system. Here we devised a sequential flash nanocomplexation (FNC) technique for the scalable production of a core–shell structured nanoparticle system by combining materials choice and particle size and structure to fulfill these functions, therefore enhancing the delivery efficiency of insulin. This method is highly effective in controlling the size, generating core–shell structure with high encapsulation efficiency (97%) and payload capacity (67%) using insulin/L-penetratin complex nanoparticles as a core coated with hyaluronic acid (HA). Both the *in vitro* and *in vivo* models confirmed that the HA coating on these core–shell nanoparticles enhanced the permeation of nanoparticles through the intestinal mucus layer and improved trans-epithelial absorption of insulin nanoparticles; and the enhancement effect was most prominent using HA with the highest average molecular weight. The insulin-loaded nanoparticles were then encapsulated into enteric microcapsules (MCs) in an FNC process to provide additional protection against the acidic environment in the stomach while allowing rapid release of insulin nanoparticles when they reach small intestine. The optimized multifunctional MCs delivered an effective glucose reduction in a Type I diabetes rat model following a single oral administration, yielding a relative bioavailability of 11% in comparison with subcutaneous injection of free-form insulin. This FNC technique is highly effective in controlling particle size and structure to improve delivery properties and function. It can be easily extended to oral delivery for other protein therapeutics.

Received 29th October 2017,
Accepted 25th January 2018

DOI: 10.1039/c7nr08047f

rsc.li/nanoscale

Introduction

Protein therapeutics is an increasingly important therapeutic modality. Due to their high susceptibility to degradation and denaturation during delivery, a wide range of nanocarriers have been developed to allow efficient packaging, enhance the stability, and improve the bioavailability of protein therapeutics, thus facilitating their delivery efficiency. Nevertheless, there is an acute shortage of methods that permit scalable production of these nanotherapeutics at high loading capacity and targeted release. We have recently developed a continuous process for producing polyelectrolyte complex NPs, termed flash nanocomplexation (FNC), in a scalable and well-controlled manner. It is particularly suitable for encapsulating water soluble, charged macromolecular therapeutics such as plasmid DNA[1] and proteins like insulin.[2] The FNC process achieves rapid and efficient mixing of two or more polyelectro-

[a]*Center for Functional Biomaterials, Key Laboratory for Polymeric Composite and Functional Materials of Ministry of Education, Sun Yat-sen University, Guangzhou 510275, P. R. China*
[b]*School of Materials Science and Engineering, Key Laboratory for Polymeric Composite and Functional Materials of Ministry of Education, Sun Yat-sen University, Guangzhou 510275, P. R. China. E-mail: chenym35@mail.sysu.edu.cn*
[c]*School of Medicine, Sun Yat-sen University, Guangzhou, 510080, P. R. China*
[d]*Department of Biomedical Engineering, Columbia University, New York, NY 10027, USA*
[e]*Department of Materials Science and Engineering, Johns Hopkins University, Baltimore, MD 21218, USA*
[f]*Institute for NanoBioTechnology, Johns Hopkins University, Baltimore, MD 21218, USA*
[g]*Department of Biomedical Engineering, Johns Hopkins University School of Medicine, Baltimore, MD 21287, USA*
[h]*Translational Tissue Engineering Center, Johns Hopkins University School of Medicine, Baltimore, MD 21287, USA*
†Electronic supplementary information (ESI) available. See DOI: 10.1039/c7nr08047f

Published on 25 January 2018. Downloaded by Columbia University Libraries on 4/28/2019 8:51:51 PM.

lyte aqueous solutions introduced by separate jet streams in a miniature mixing-chamber. It generates a suspension of polyelectrolyte NPs stabilized by residual charges on particle surface. Comparing with bulk mixing or drop-wise addition, this FNC method offers several unique advantages like controllable NP size, narrow size distribution, and higher encapsulation efficiency and loading level for therapeutic payloads. We have applied the FNC process to prepare insulin/chitosan NPs with an average size range of 45 to 115 nm controllable through adjusting the flow rate of FNC jet streams. When loaded in enteric capsules, the 45 nm NPs showed higher trans-epithelial transport than larger NPs, and yielded higher insulin delivery efficiency and efficacy in lowering blood glucose level in a Type I diabetes rat model.[2]

Oral administration has been considered as a preferred delivery method for insulin in order to manage blood glucose level for treating patients suffering from diabetes mellitus, due to better patient compliance and noninvasive nature of the administration route.[3,4] The current treatment option requires daily subcutaneous injection (s.c.) of insulin, which is associated with side effects such as hyperinsulinemia and lipoatrophy.[5,6] Orally delivered insulin is directly transported into the hepatic portal circulation upon uptake through the small intestine, thus imitating the physiological route of insulin secretion. Nanoparticles (NPs) formed *via* polyelectrolyte complex of charged polymers such as chitosan, *N*-trimethyl chitosan, polypeptides, poly(amino acid)s, poly(acrylic acid), alginate, dextran, hyaluronic acid, and their derivatives offer significant protection to the encapsulated insulin in the gastrointestinal (GI) tract, thus improving the delivery efficiency across the small intestinal epithelium.[7,8] However, the oral bioavailability and pharmacodynamic performance of current insulin-loaded NP systems are still far from satisfactory. Two of the remaining key barriers are limited efficiency of NPs passing through the mucus layer and accessing apical surface, and poor transcellular transport into the systematic circulation.[9–13] Potential strategies to overcome the mucus layer and absorption barrier of intestinal epithelium may include incorporating permeation enhancers, reducing NPs size, and modulating the surface charges, therefore improving bioavailability of orally delivered insulin.[14–17]

L-Penetratin is a cell-penetrating peptide (CPP) acting as a trans-epithelial transport enhancer. Its positively-charged nature allows it to complex with negatively charged protein to construct nanocomplexes for oral delivery.[15,18–20] Hyaluronic acid (HA), a natural polyanion exhibiting excellent biocompatibility and biodegradability, has been shown to reduce interaction of the NPs with mucin network and to improve NP transport in the mucus layer.[21–23] Herein, we utilized these properties to prepare CPP/insulin NPs using FNC method, and used it as a core for additional coating with HA in an FNC process to generate a core/shell NP (Scheme 1, NP-B) to achieve both excellent mucus permeation and trans-epithelial absorption properties. As previous reported, fabrication of protein-loaded enteric capsules is inefficient because of the multi-step process.[24–26] Here we further explored the feasibility of using FNC platform to generate the microcapsule (Scheme 1, MC) to confer pH-sensitive property for protecting NPs in the gastric environment and site-specific release of NPs in the intestinal tract. We used insulin as a model protein drug with the goal to develop scalable production plus sequential coating processes for preparing protein-loaded core–shell NPs.

Experimental

Penetratin peptide (Ste-RQIKIWFQNRRMKWKK) was chemically synthesized by Nanjin Taiye Biopharmaceuticals Co., Ltd (Jiangsu, China). Porcine insulin (27.4 IU mg^{-1}) was purchased from Wanbang Bio-Chemical Co., Ltd (Jiangsu, China). Sodium hyaluronate with three different M_w (weight average M_w = 4.7, 35, 190 kDa) were obtained from Freda

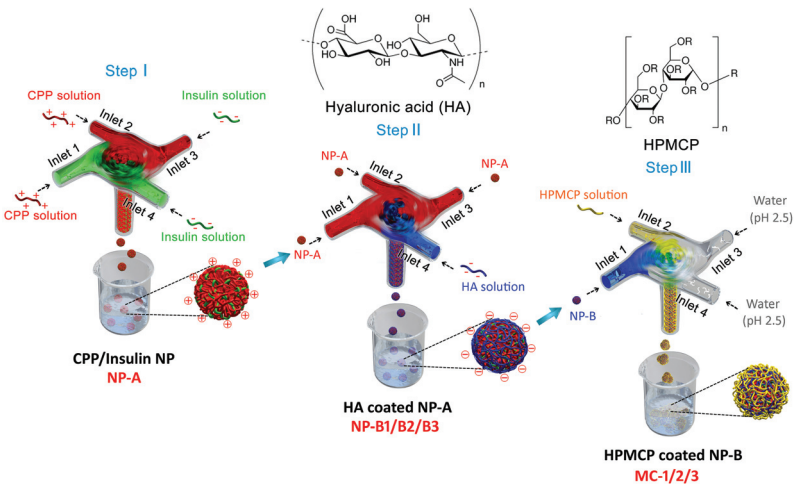

Scheme 1 Schematic representation of sequential FNC platform for preparation of the CPP/insulin nanoparticle (NP-A) core, HA-coated NPs (NP-B1/B2/B3) and HPMCP coated NP-B (MC-1/2/3).

 This journal is © The Royal Society of Chemistry 2018

Published on 25 January 2018. Downloaded by Columbia University Libraries on 4/28/2019 8:51:51 PM.

Pharmaceutical Co. Ltd (Shangdong, China). Fluorescein isothiocyanate (FITC), Rhodamine B isothiocyanate (RITC) and Rhodamine 123 (Rho123) and were purchased from Aladdin (Shanghai, China). Sulfo-cyanine 5-NHS (Cy-5) ester and sulfo-cyanine 3-NHS (Cy-3) ester was purchased from Little-PA Sciences Co., Ltd (Wuhan, China). Alexa Fluor® 647 conjugate of wheat germ agglutinin (AF-647), 4′,6-diamidino-2-phenylindole (DAPI) and 3-(4,5-dimethyl-thiazol-2-yl)-2,5-diphenyl tetrazolium bromide (MTT) were purchased from Abcam (UK). Porcine insulin ELISA kit was purchased from Mercodia Inc. (Sweden). Alkaline phosphatase (ALP), aspartate transaminase (AST), alanine aminotransferase (ALT) and γ-glutamyl transpeptidase (γ-GT) assay kits were purchased from Jiancheng Biotech. Co. Ltd. All chemical reagents utilized in this study were analytic grade.

Preparation and characterization of NPs

L-Penetratin was dissolved to a concentration of 0.3 mg mL^{-1} in double distilled water (ddH_2O). The pH of the CPP solution was adjusted to 5.0–8.0 by 3 M sodium hydroxide (NaOH). Insulin was dissolved in hydrochloric acid aqueous solution (0.01 M HCl) at a concentration of 1.0 mg mL^{-1} and then the pH was adjusted to 6.8 using 3 M NaOH. Sodium hyaluronate with three different M_w at 4.7, 35, 190 kDa was dissolved in ddH2O at a concentration of 0.7, 0.3, 0.28 mg mL^{-1}, respectively. L-Penetratin is a polycationic peptide that possesses strong affinity and readily complex with negatively charged insulin to form CPP/insulin NPs which was termed as NP-A. The positively charged NP-A and negatively charged HA were further assembled to form NPs with NP-A core surrounded by HA coating which was termed as NP-B, as shown in Scheme 1. NP-B prepared with three different HAs (M_w: 4.7, 35, 190 kDa) were termed accordingly as NP-B1, NP-B2, and NP-B3.

The NPs were characterized for size and zeta potential with a Malvern Zetasize NanoZS90 (Malvern Instruments Ltd, UK). The morphology of NP-A/NP-B/MC were examined by transmission electron microscope (TEM, JEOL-1400, Japan). To evaluate the encapsulated efficiency (EE) and drug loading content (LC), NP-A or NP-B suspension was pipetted into the ultrafiltration tube (molecular weight cutoff at 100 kDa), followed by centrifugation at 1500*g* for 20 min at 4 °C. After centrifugation, the amount of free RITC-insulin in the filtrate of fluorescence-labeled NPs was measured by Multi-Mode Microplate Reader (Biotek, US). To evaluate the EE of HPMCP-coated microcapsule (termed MC) suspension was pipetted into the centrifugal tube, followed by centrifugation at 8000*g* for 20 min at 4 °C. After centrifugation, the amount of free RITC-insulin in the supernatant of fluorescence-labeled NPs was measured by Multi-Mode Microplate Reader. To further investigate the interaction between insulin and HA, FRET analysis was performed. Rho-123 (ex: 490 nm, em: 530 nm) and RITC (ex: 540 nm, em: 580 nm) were used as FRET pairs. Labeled NP-B nanoparticles were prepared by using RITC-labeled insulin or/and Rho 123-labeled HA using the same procedure as described above. The fluorescence intensity was measured through a fluorescence spectrophotometer (Edinburgh Instruments FS-980, UK) with an excitation wavelength of 450 nm and the emission spectrum was recorded from 500 to 700 nm.

NPs stability and mucin aggregation study

For the measurement of NPs stability, freshly prepared NPs were placed at 4 °C and 25 °C. The particle size and PDI was determined by dynamic light scattering (DLS) measurement after different time intervals (1, 3, 6, 9, 12, 18, 24, 48 h). For the measurement of NP–mucin interaction, freshly prepared RITC-labeled NPs were dispersed in mucin solution of different concentration of 0.5%, 1.0% (m/v), vortexed and incubated for 1 h at 37 °C in a shaker. The mixture was centrifuged at 3000*g* for 10 min and the precipitates were washed with PBS twice. Subsequently, the precipitates were disintegrated with 200 μL of NaOH (3 M) thoroughly; the mixtures were incubated for 10 min, and the fluorescence intensity was measured by Multi-Mode Microplate Reader.

Lyophilization of nanoparticles

All tested NP-B1/2/3 were added to 2% sorbitol (w/v) solution and aliquoted into glass vials. The solution was snap-frozen by immersion in liquid nitrogen for 10 min and lyophilized using an Alpha 1–2 LD Plus lyophilizer (Martin Christ Inc., Osterode, Germany) at −30 °C and 0.37 mbar for 36 h, followed by a secondary drying step at 0 °C and 6.1 mbar for 12 h. Size distribution and insulin leakage were analyzed after reconstitution of freeze-dried NPs in distilled water.

In vitro release profile of insulin-loaded nanoparticles

The loss of insulin at pH 2.5 (HCl solution) and pH 7.0 (10 mM PBS with hyaluronidase 0.01 mg mL^{-1}), simulating the pH environments in fasting stomach and upper small intestine were analyzed at 37 °C under agitation (100 rpm). The *in vitro* release profile of insulin of the tested NPs in PBS (pH 7.4) with or without hyaluronidase was analyzed at 37 °C under agitation (100 rpm). At various time points, the NPs were removed by ultrafiltration (molecular weight cutoff at 100 kDa), and the filtrate were assayed for insulin using fluorescence detection by Muti-Mode Microplate Reader.

Cell culture

Caco-2 and HT29-MTX cells were cultivated separately in tissue culture flasks using Dulbecco's modified Eagle's medium (DMEM) supplemented with high glucose, 10% fetal bovine serum, 1% nonessential amino acids, 1% L-glutamine, 1% penicillin and streptomycin (100 IU mL^{-1}). Both cells were cultured in growth medium at 37 °C in a 5% CO_2 incubator. For the cytotoxicity assay, HT29-MTX cells (1.0×10^4 cells per well) were seeded into 96-well plates.

Mucus permeation studies

For the permeation study in mucus layer, HT29-MTX cells were seeded at a density of 2.0×10^4 cells per well into a glass-bottom dish (1 cm × 1 cm), and then incubated with fluorescence labeled NPs (Cy5-labeled insulin, FITC-labeled CPP)

Published on 25 January 2018. Downloaded by Columbia University Libraries on 4/28/2019 8:51:51 PM.

for 3 h, which was followed by a thorough washing process to remove the remaining mucus and the surface attached samples. Then, the cells were fixed with 4% cold paraformaldehyde for 15 min and washed with PBS. For the visualization of the cell monolayer, the cell nucleus was stained with DAPI (blue). The samples were observed under confocal microscopy.

Intracellular uptake studies

For the study of intracellular uptake, Caco-2 or HT29-MTX cells were seeded into 24-well plates (5.0×10^4 cells per well). Both mucus-containing (HT29-MTX) and mucus-free (Caco-2) cells were then incubated with RITC-labeled NPs (RITC-labeled insulin) for 3 h, which was followed by a thorough washing process to remove the remaining mucus and the surface attached samples. Then, the cells were lysed, and the cell-associated fluorescence intensity was measured using Multi-Mode Microplate Reader. The relative amount of uptake was corrected using the cell number account measured by the Scepter™ 2.0 handheld automated cell counter. The uptake of NPs was also evaluated on Caco-2/mucin model. Mucin was added into the culture medium to simulate the presence of mucus layer which was covered on the epithelia.

Trans-epithelial transport investigation

For the establishment of *in vitro* cell monolayer, the Caco-2 cells were seeded at a density of 2.0×10^4 cells per well on a polyester membrane (0.4 μm in pore size, diameter 12 mm, 1.1 cm^2 of cell growth area) in Costar Transwell 12 wells per plate (Corning) and cultured for 2–3 weeks. Culture medium in both upper and bottom compartments were changed every two days. The trans-epithelial electrical resistance (TEER) was measured with an electrical resistance meter (Millcell ERS-2, Millipore) to monitor the integrity of cell monolayer. The cell monolayers with TEER values in the range of 600–800 Ω cm^{-2} were used for the experiment. Then medium in apical chamber was replaced by 200 μL of fresh serum-free medium with RITC-labeled NPs (RITC-Insulin concentration: 0.2 mg mL^{-1}). To investigate the influence of mucus on insulin loaded NPs permeation, experiments were also performed in a Caco-2/mucin model as a counterpart which apical chamber containing 10 mg mL^{-1} of mucin. After 4 h incubation, the RITC-insulin concentration in basolateral medium was determined and the Papp value was calculated accordingly.

$$P_{app} = Q/A \cdot c \cdot t \quad (1)$$

where Q is the total amount of insulin permeated (ng), A is the diffusion area of the cell monolayers (cm^2), c is the initial concentration of the insulin in the donor compartment (ng cm^{-1}) and t is the total time of the experiment (s).

Structural changes of NPs

For the observation of structural changes of NPs, HT29-MTX cells were seeded at a density of 2.0×10^4 cells per well into a glass-bottom dish (1 cm × 1 cm), and then incubated with fluorescence labeled NPs (Cy5-labeled insulin, RITC-labeled HA) for 2 h, which was followed by a thorough washing process to remove the remaining mucus and the surface attached samples. Then, the cells were fixed with 4% cold paraformaldehyde for 15 min and washed with PBS. For the visualization of the cell monolayer, the cell nucleus was stained with DAPI (blue). The samples were observed under confocal microscopy.

Animal study

All animals were purchased from the Animal Experimental Center in Guangzhou (Guangzhou, China). Animals received care in compliance with the guidelines outlined in the Guide for the Care and Use of Laboratory Animals and national regulations. All of the experimental procedures had been conducted following a protocol approved by the Institutional Animal Care and Use Committee of Sun Yat-sen University (SYSU).

In vivo fluorescence imaging of absorption study

In vivo absorption study in rats were performed with Cy3-insulin to visualize its absorption performance in the small intestinal villi. Male SD rats weighing between 230 and 250 g were fasted overnight (~8 h) before experiments with free access to water. All the tested insulin formulations (Cy3-labeled insulin, insulin dose: 1.5 mg kg^{-1}) were administered by oral gavage. After 2 h, the rats were euthanized with pentobarbital sodium (0.04 mg kg^{-1}). The intestinal tissue (jejunum) were removed, longitudinal cut along the direction of lumen, and then mildly washed with PBS. Next, the tissue of jejunum was rolled up and frozen quickly in liquid nitrogen-cooled OCT-compound. The tissue was cross-sectioned and stained with Alexa Fluor 647-conjugated Wheat germ agglutinin (AF 647) and DAPI to visualize the mucus layer and nucleus, respectively. The tissue-sections were observed by confocal microscopy.

In vivo hypoglycemic effect and pharmacokinetics

The hypoglycemic effect and pharmacokinetic of the tested NPs following oral administration were evaluated on Type 1 diabetic rats. For the Type 1 diabetic model induction, male SD rats weighing 230–250 g were intraperitoneal (i.p.) injected with streptozotocin (STZ, 70 mg kg^{-1}). Animals were considered to be diabetic if they exhibited fasting blood glucose level over 16.0 mM at 1 week after the injection. The rats were fasted overnight but allowed free access to water prior to the experiment. Free insulin solution and different NPs following administration at a dose of 80 IU kg^{-1} *via* gavage and free insulin solution following subcutaneous (s.c.) injection at dose of 5 IU kg^{-1}. Likewise, different HPMCP-coated NP-B insulin formulations (*i.e.* MCs) were given *via* oral gavage at a dose of 80 IU kg^{-1}. Oral gavage administration was performed using an oral gavage tube (i.d. 0.9 × 50 mm in length). Blood glucose level was determined using a glucose meter (OneTouch® UltraVue, Johnson). Blood samples were collected from the tail veins prior to the administration and at different time intervals after the administration. Serum insulin levels were quantified using porcine insulin ELISA kit. The area under the curve of

 This journal is © The Royal Society of Chemistry 2018

Published on 25 January 2018. Downloaded by Columbia University Libraries on 4/28/2019 8:51:51 PM.

serum insulin concentration was calculated. The pharmacological availability (PA) and the bioavailability (BA) relative to s.c. injection was analyzed as following equations:

$$\mathrm{PA}\,(\%) = \frac{\mathrm{AAC_{oral}} \times \mathrm{Dose_{s.c.}}}{\mathrm{AAC_{s.c.}} \times \mathrm{Dose_{oral}}} \times 100 \quad (2)$$

$$\mathrm{BA}\,(\%) = \frac{\mathrm{AUC_{oral}} \times \mathrm{Dose_{s.c.}}}{\mathrm{AUC_{s.c.}} \times \mathrm{Dose_{oral}}} \times 100\% \quad (3)$$

whereas AAC_{oral} and $AAC_{s.c.}$ are the areas above the curves of blood glucose levels in the percentage change *versus* time for 0–8 h of oral gavage and s.c. injection, respectively; AUC_{oral} and $AUC_{s.c.}$ represent the total area under the curves of serum insulin concentration *versus* time for 0–8 h of oral gavage and s.c. injection, respectively; $Dose_{oral}$ and $Dose_{s.c.}$ represent the dose of insulin used of oral gavage and s.c. injection, respectively.

Toxicity study

To investigate whether long-term orally administration of the NP-B and NP-B loaded microcapsules (MCs) causes the unwanted side effect, four of the liver function indicators (ALP, AST, ALT, γ-GT) were monitored by using assay kit after 7 days of consecutive administration (80 IU kg^{-1} day^{-1}). For histopathology study, the samples fixed in formalin were dehydrated by an ascending alcohol series ending in xylol and finally embedded in paraffin. The tissue samples were sectioned at a thickness of 4–6 μm and sections were stained with hematoxylin–eosin (H&E), then the tissue-sections were observed under light microscopy (200×).

Statistical analysis

All values are expressed as mean ± SD. Comparisons among all groups were performed using One-way ANOVA or *t*-test by GraphPad Prism version 5.0 for Windows (GraphPad Software, USA), and $p < 0.05$ is considered statistically significant.

Results and discussion

Polyelectrolyte complexation as a facile ionic-gelation process occurring in aqueous media has been adopted for preparing NPs to encapsulate charged water-soluble therapeutic agents such as proteins and nucleic acids.[1,2,27–29] It has also been widely used to achieve electrostatic charge-mediated layer-by-layer coating of the surface of nanoparticles, as it may improve the stability and the bioactivity of these particulates for delivery purpose. For example, HA can be coated onto particle surface to reduce aggregation of NPs for drug and gene delivery *via* intravenous (i.v.) delivery.[10,30–32] Such a polyelectrolyte coating can enhance *in vivo* pharmacodynamics performance by improving NP characteristics such as stability and pharmacokinetic profiles. To improve the delivery efficiency through oral administration, NPs can be filled into pH-sensitive enteric capsules to protect the therapeutic protein payload in the gastric cavity, and to specifically deliver the drug to small intestine.[24,26,33] Traditionally, the polyelectrolyte complexation in NPs preparation and surface coating are achieved through manual bulk mixing, vortex, or drop-wise addition, which suffer from poor reproducibility in scale-up production and limited control over the NP quality in terms of size, uniformity and colloidal stability. They also hinder the scale-up production of NPs carrying biologics for clinical translation.[34–37]

FNC platform setup for preparation of insulin-loaded core–shell nanoparticles

A four-stream multi-inlet vortex mixer (MIVM) device was constructed based on a reported design.[38,39] The insulin loaded core–shell NPs were prepared through a three-step process based on the FNC platform (Scheme 1). Firstly, L-penetratin, a polycationic CPP with 16 amino acids, was applied to form CPP/insulin NPs (NP-A) by charge interaction with insulin. However, the formed NPs were not stable and aggregated easily. L-Penetratin was then modified by grafting a stearoyl group to the N-terminal arginine residue to increase hydrophobicity for stabilizing NP-A. Next, HA was coated onto the NP-A core to form NP-B with a core–shell structure. We hypothesized the HA coating could gradually dissociate from the NP-A core during mucosal permeation, thus delivering intact CPP/insulin nanoparticles (NP-A) to the apical surface of the epithelium. Finally, an enteric material, hydroxypropylmethyl cellulose phthalate (HPMCP),[25] was coated onto NP-B NPs to form microcapsules (MC) for preserving the nanostructure and protein activity in the harsh environment of the stomach.

In Step I, a solution of stearoyl L-penetratin was introduced through Inlet 1 and Inlet 2, and insulin solution through Inlet 3 and Inlet 4. The obtained NP-A with positive charge on the surface was then introduced to another FNC device to mix with negatively charged HA to generate HA-coated NPs (NP-B, Step II). The NP-A solution was introduced through Inlet 1, 2, and 3, and HA solution through Inlet 4. In Step III, the NP-B was coated with HPMCP (HP 55), a pH-sensitive polymer commonly used as an enteric coating for oral dosage forms. NP-B suspension was re-introduced into the third FNC device through Inlet 1, HPMCP solution through Inlet 2, and diluted hydrochloric acid solution (pH 2.5) through Inlet 3 and Inlet 4. Water was applied as the media of all solutions. To keep the optimization process simpler, all inlets were running at the same volumetric flow rate controlled by programmable digital syringe pumps.

Optimization and characterization of insulin-loaded NP core (NP-A), HA-coated NPs (NP-B), and HPMCP-coated microcapsule (MC)

In Step I for NP-A preparation, the two crucial parameters for particle formation and size control include the initial pH of CPP solution and volumetric flow rate of the solution streams introduced into the MIVM. While the concentration (1.0 mg mL^{-1}), the pH of insulin (pH 6.8) and the flow rate (30 mL min^{-1}) were kept constant, the pH of CPP solution (0.3 mg mL^{-1}) was optimized. As shown in Fig. 1a, the initial pH of the CPP solution significantly influenced its ionic nature, thus

Published on 25 January 2018. Downloaded by Columbia University Libraries on 4/28/2019 8:51:51 PM.

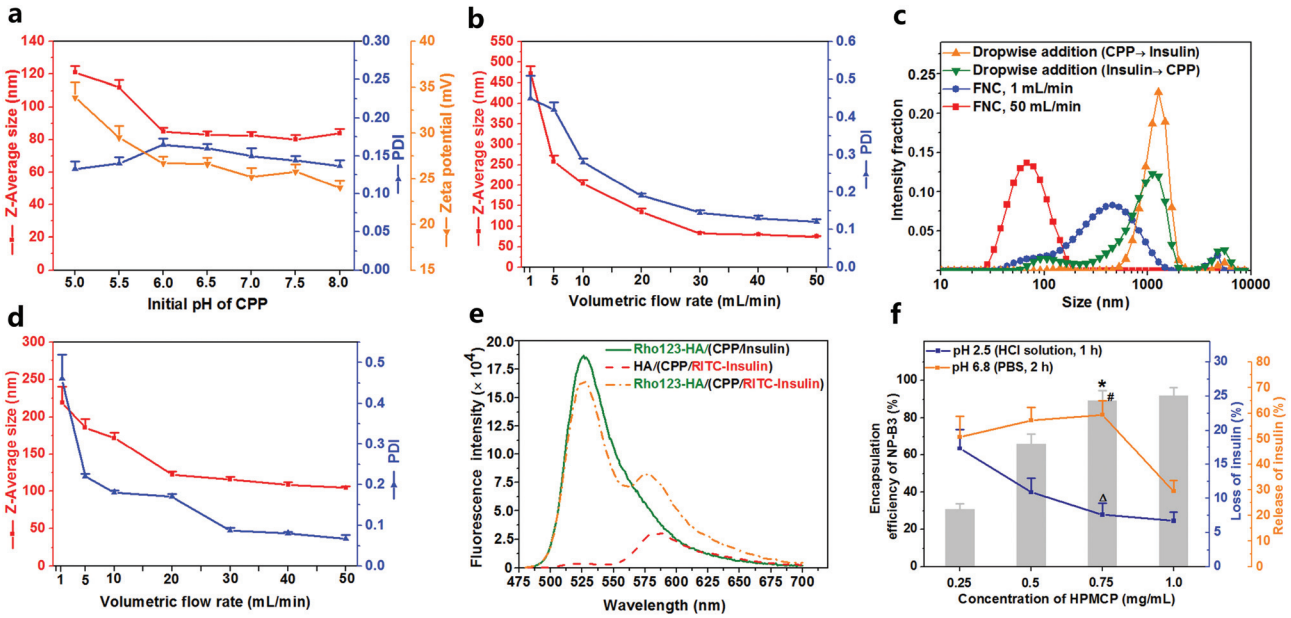

Fig. 1 Optimization and characterization of insulin formulations. (a) Effect of initial pH of the CPP solution on size, PDI, and zeta potential of CPP/insulin nanoparticle (NP-A) core. Conditions used: CPP solution, 0.3 mg mL^{-1}, pH 5.0–8.0; insulin solution, 1 mg mL^{-1}, pH 6.8; flow rate for all channels, 30 mL min^{-1}. (b) Effect of volumetric flow rates (VFR, 1–50 mL min^{-1}) on particle size and PDI of NP-A. Conditions used: CPP solution, 0.3 mg mL^{-1}, pH 8.0; insulin solution, 1 mg mL^{-1}, pH 6.8. (c) Size distribution of NP-A prepared by different methods. Conditions used: CPP solution, 0.3 mg mL^{-1}, pH 8.0; insulin solution, 1 mg mL^{-1}, pH 6.8. (d) Effect of VFR (1–50 mL min^{-1}) on particle size and PDI of the NP-B3, which possessed a NP-A core with HA (M_w: 190 kDa) coating. (e) Emission spectrum of NP-B3 with only HA labelled by Rho123 (green solid line), NP-B3 with only insulin labelled by RITC (red dashed line), and NP-B3 with both HA labelled by Rho123 and insulin labelled by RITC (yellow dot dash line), with excitation at 450 nm. (f) Effect of HPMCP concentration on the encapsulation efficiency and pH-sensitive release profiles of HPMCP-coated NP-B3 (*i.e.* MC-3). $^{*}p < 0.001$ *vs.* 0.25 mg mL^{-1} or 0.5 mg mL^{-1} group; $^{\#}p < 0.001$ *vs.* 1.0 mg mL^{-1} group; $^{\Delta}p < 0.001$ *vs.* 0.25 mg mL^{-1} group. Data are shown as means ± SD (n = 6).

affecting the size and surface charge (*i.e.* zeta potential) of NP-A. As the pH of the CPP solution increased from 5.0 to 6.0, the average size of the NPs decreased from 120 nm to 85 nm; further increasing of the pH did not change the average size significantly. The polydispersity index was maintained around 0.15 for all conditions tested. The zeta potential of the NP-A decreased with increase of pH but remained constant at around +24 mV in the range of pH 6.0–8.0. The volumetric flow rate directly influenced the mixing efficiency inside the chamber, and thus NP size and size distribution. Under optimized concentrations of CPP (0.3 mg mL^{-1}, pH 8.0) and insulin (1.0 mg mL^{-1}, pH 6.8), the average size of NP-A was tuned from 472 nm to 75 nm as the volumetric flow rate increased from 1.0 mL min^{-1} to 50 mL min^{-1} (Fig. 1b and S1†).

To demonstrate the advantages of FNC process, conventional drop-wise addition method was also applied to prepare NP-A for comparison. The NPs were made by either adding an aqueous solution of insulin into an aqueous solution of CPP or *vice versa* under mild agitation. The NPs prepared in either way exceeded 1 μm in size, which then precipitated within 1 h. In contrast, the NP-A prepared by FNC method under optimized flow rate (50 mL min^{-1}) had an average size of 75 nm with a PDI of 0.12 (Fig. 1c).

Surface coating technology, driven by the electrostatic interaction between polyelectrolytes and an oppositely charged substrate, is a well-acknowledged technique for the solution-phase preparation of multifunctional nanoscale therapeutics.[10,40,41] To generate NPs with homogeneous surface coating in continuous and scalable manner is still a bottleneck, which limits the development of surface decoration of nano-formulations. HA is a negatively charged biodegradable polysaccharide.[23] We examined the relationship between the HA molecular weight M_w and HA coating efficiency and stability of the nanoparticles. The NP-A core was coated with the HA with an average M_w of 4.7 kDa, 35 kDa and 190 kDa, generating NP-B1, NP-B2 and NP-B3, respectively. In Step II (Scheme 1), similarly as the Step I, the average size of the NP-B can be varied from 219 nm to 103 nm by adjusting the flow rate from 1 to 50 mL min^{-1}, while the PDI decreased from 0.46 to 0.067 (Fig. 1d). HA-coated nanoparticles prepared under flow rates lower than 1 mL min^{-1} exhibited poor colloidal stability.

The coating of HA was further validated using a fluorescence resonance energy transfer (FRET) analysis. The NP-B3 was prepared with Rho123-labeled HA (Rho123-HA) and RITC-labeled insulin (RITC-insulin), which can form a FRET pair. The emission intensity of Rho123-HA decreased at 530 nm and that of RITC-insulin increased at 580 nm, which implied significant energy transfer from donor to acceptor (Fig. 1e), confirming the effective coating of HA on insulin-loaded NP-A. These results collectively demonstrated that the FNC process is

 This journal is © The Royal Society of Chemistry 2018

Published on 25 January 2018. Downloaded by Columbia University Libraries on 4/28/2019 8:51:51 PM.

an effective method for nanoparticle coating through charge-mediated complexation, and the flow rate of each stream is a critical parameter to control the coating efficiency and size of the NPs.

Using the flow rate of 50 mL min^{-1}, we prepared three HA-coated NP samples, NP-B1, NP-B2, and NP-B3, respectively. As shown in Table 1, the resultant NP-B1/2/3 possessed a negative zeta potential of around −20 mV, and their size increased to approximately 100 nm. The reversal of surface charge and the size increase indicated successful coating of anionic HA on the outer surface of the NP-B. We expected that these NP-B of sub-200 nm in diameter could meet the steric requirement for primarily rapid diffusion through lower viscosity pores within the elastic matrix. And it is noteworthy that all three NP-B1/2/3 samples exhibited very high encapsulation efficiency (>95%) and drug loading content (>55%).

In Step III (Scheme 1), the NP-B was further encapsulated with HPMCP as an enteric microcapsule shell. HPMCP was dissolved in ethanol/water (7/3, v/v) and introduced into MIVM to microencapsulate NP-B under acidic pH environment. The size of NP-B NPs was stable upon challenged by the solvent and pH used (data not shown). The encapsulation efficiency of NP-B in MCs increased with the concentration of HPMCP and reached a plateau of 90% when HPMCP was at a concentration of 0.75 mg mL^{-1}. Rapid release of NPs from MCs could be achieved at pH 6.8 (Fig. 1f). Further increasing the concentration of HPMCP significantly slowed down the release of NPs. Therefore, we selected this concentration of HPMCP (0.75 mg mL^{-1}) as the optimal condition to generate the enteric MCs for the following experiments.

The core component of the FNC process is the mixing chamber with a small and defined volume that we adopted from an MIVM design in the FNP method.[38,42,43] This chamber ensures efficient mixing of the multiple incoming streams when infused at high flow rates. Consistent with the typical FNP process, as the flow rate increases, the flows gradually become chaotic and ensure a turbulent-like mixing pattern inside the chamber.[1,2] Comparing with a low flow rate (*e.g.* 1 mL min^{-1} for each inlet), a smaller size and a more uniform size distribution can be obtained in a high flow rate (*e.g.* 30 mL min^{-1}). Notably, a high flow rate is essential to achieve sufficient coating in Step II and a high encapsulation efficiency in Step III using the FNC platform. We attribute this to the assumption that a turbulent mixing pattern can expose NP-A surfaces to HA and expose NP-B surface to HPMCP in a homogenous manner.

The morphology of all tested NPs and MCs were visualized by TEM as shown in Fig. 2. NP-A NPs are spherical in shape with an average size of 80.7 ± 9.9 nm (n = 50), matching the size measured from DLS. After coating with HA, the average sizes of NP-B1, NP-B2 and NP-B3 were 86.5 ± 9.5 nm (n = 50), 118.4 ± 12.7 nm (n = 50) and 178.9 ± 21.3 nm (n = 50), respectively. These images also revealed a clear core–shell structure. In the third step, the average size of spherical MCs with an HPMCP coating increased even more obviously. For example, MC-3 reached 1.3 ± 0.1 μm (n = 50). The MC of such a big size may encapsulate more than one NP-B particles.

The storage stability of the NP-A and NP-B was investigated by monitoring the size and PDI at 4 °C or 25 °C. At 4 °C, NP-A and NP-B NPs were stable for at least 1 month. At 25 °C, the size of NP-A increased progressively whereas that of NP-B remained stable, suggesting good storage stability for the HA-coated NPs (Fig. 2f). Meanwhile, we identified the 2% sorbitol (w/v) as an effective cryoprotectant for NP-B (Table S1†). It is worth noting that the lyophilization process had no influence on the average size and surface charge of NP-B nanoparticles, and the encapsulation efficiency of insulin upon reconstitution remained the same.

To sum up, by the above sequential procedure, multifunctional and core–shell NPs carrying insulin were generated by FNC in a continuous and scalable manner. The structure of NPs can be tailored by changing the concentration of substrates, the pH, the flow rate, *etc*. Using this sequential FNC device and process, the total output of 190 kDa HA-coated NP-B3 at a flow rate of 50 mL min^{-1} was 6.6 g h^{-1}, which corresponds to 4.5 g h^{-1} of insulin dose.

In vitro release of insulin and mucin affinity

The release profiles of encapsulated insulin from NP-A and NP-B in PBS (10 mM, pH 7.4) at 37 °C with hyaluronidase are shown in Fig. 2g and S2.† The sustained release profiles of NP-B2 and NP-B3 within 12 h were observed while uncoated NP-A displayed a much faster release during the first 2 h. These results confirmed the protection provided by the outer HA coating. In addition, as shown in Fig. S3,† there was no significantly insulin loss for NP-B in a simulated gastric fluid (pH 2.5) and a simulated small intestinal fluid (pH 7.0).

The negatively-charged mucin in mucus layer can bind to positively charged NP-A surface. Thus, the mucus layer covering the epithelium presents a barrier for local permeation of insulin loaded NP-A at mucosal surface. We hypothesized that by shielding the positive charge on NP-A core with HA coating,

Table 1 Characterization of NP-A and NP-B nanoparticle formulations

Nanoparticles	M_w of HA	Con. (mg mL^{-1})	Average size[a] (nm)	Zeta potential[a] (mV)	PDI[a]	EE[a] (%)	LC[a] (%)
NP-A	—	—	75.7 ± 2.7	22.5 ± 0.8	0.12 ± 0.01	93.9 ± 1.6	75.8 ± 0.3
NP-B1	4.7 kDa	0.7	102.9 ± 4.6	−18.6 ± 0.7	0.06 ± 0.02	95.6 ± 2.4	55.5 ± 0.6
NP-B2	35 kDa	0.3	101.2 ± 4.3	−19.5 ± 0.5	0.07 ± 0.01	97.3 ± 1.8	66.1 ± 0.4
NP-B3	190 kDa	0.28	103.7 ± 3.5	−19.7 ± 0.6	0.07 ± 0.02	96.6 ± 1.7	66.7 ± 0.5

[a] Data are shown as means ± SD (n = 6).

Published on 25 January 2018. Downloaded by Columbia University Libraries on 4/28/2019 8:51:51 PM.

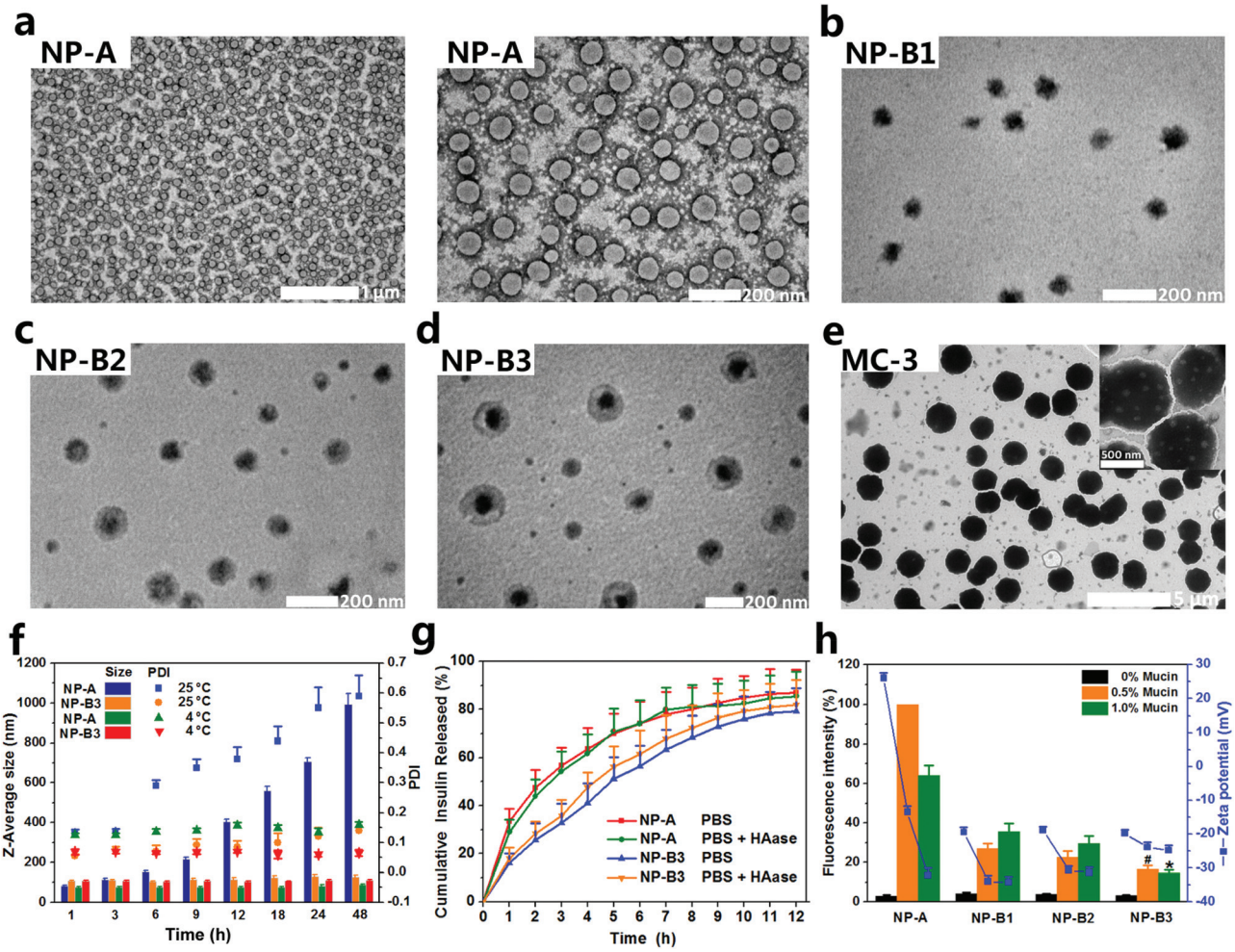

Fig. 2 (a–e) TEM images of different nanoparticle formulations. (a) CPP/insulin NP-A, (b) HA (M_w 4.7 kDa)-coated NP-A (NP-B1), (c) HA (M_w 35 kDa)-coated NP-A (NP-B2), (d) HA (M_w 190 kDa)-coated NP-A (NP-B3), and (e) HPMCP-coated NB-3 (MC-3). (f) Stability of NP-A and NP-B3 suspensions at 4 °C and 25 °C. Data are shown as means ± SD (n = 6). (g) *In vitro* release profiles of insulin from NP-A and NP-B3 in PBS (pH 7.4) with or without hyaluronidase (0.01 mg mL^{-1}). Data are shown as means ± SD (n = 4). (h) Percentage of particle–mucin aggregation formed in mucin solution at different concentration for NP-A and NP-B nanoparticles within 1 h at 37 °C. The fluorescent intensity of aggregates for NP-A at 0.5% mucin is referenced as a background control and normalized to 100%; $^{\#}p < 0.01$ *vs.* all other groups at 0.5% mucin; $^{*}p < 0.001$ *vs.* all other groups at 1.0% mucin. Data are shown as means ± SD (n = 4).

the resultant NP-B would have low interaction with the mucus layer. To test this hypothesis, we monitored the interaction between NP-A or NP-B1-3 with mucin by measuring the amount of NP-mucin aggregates formed in various concentrations of mucin. As shown in Fig. 2h, significantly lower levels of aggregation were observed in all three NP-B samples compared with the uncoated NP-A. For instance, at a mucin concentration of 0.5% and 1.0% (w/v), the aggregates formed in NP-B3 group were only 16.5% and 22.9% of NP-A, respectively. Surprisingly, more aggregation was observed in NP-A group at 0.5% of mucin than that of a higher mucin concentration (1%). We speculated that this was caused by the instability of the nearly electro-neutral surface charged (−13 mV) NP-A-mucin (0.5%) aggregates. Since all NP-B1/2/3 nanoparticles with HA coating possess negative surface charge and hydrophobic or electrostatic interactions with mucin is avoided.

In vitro mucus permeation ability of NP-A and NP-B

The mucus barrier that covering the GI tract is the main cause of low protein oral bioavailability.[9,11,44] In addition, trans-epithelial transport poses another challenge for sufficient absorption into the systematic circulation. Theoretically, the charge reversal caused by HA coating reduces mucin adsorption by electrostatic repulsion; and the hydrophilicity offered by this HA coating enhances the NP motion and transport through the mucus layer. However, the negatively charged HA coating does not favor trans-epithelial transport. It is therefore critical to make the HA coating persist long enough to facilitate the NP transport through the mucus layer, and yet at the same

 This journal is © The Royal Society of Chemistry 2018

Published on 25 January 2018. Downloaded by Columbia University Libraries on 4/28/2019 8:51:51 PM.

time, detach at the appropriate site close to the apical surface of the epithelium to deposit the NP-A core onto the epithelium cells.

We selected HT29-MTX cell line, which can continuously produce mucin, as a cell culture model to simulate mucosal transport.[9,28] As indicated by MTT assay, all tested insulin formulation exhibited no significant cytotoxicity on the HT29-MTX cells at the concentration from 10 to 250 μg mL^{-1} (Fig. S4†). To verify the behavior of the NP-A and NP-B as they permeated through the mucus layer, the distribution of different components of NP-A or NP-B on HT29-MTX cell monolayer was observed using confocal laser scanning microscopy (CLSM). As shown in Fig. 3a, after 3 h of incubation with soluble Cy5-insulin, low fluorescence signal was observed at a deeper depth of observation (30 μm). On the contrary, fluorescence signal (red) from Cy5-insulin was well appreciated at that depth in both NP-A and NP-B groups (image of NP-B2 group was shown in Fig. S5†). Besides, there were massive entrapments of fluorescence signal at two upper depths (0 and 15 μm) for the groups of free insulin, NP-A and NP-B1. These findings support the above results of mucin affinity *in vitro*. This NP-A/NP-B interception in the mucus layer could be improved by coating HA of a higher M_w. As expected, the Cy-5 insulin fluorescence intensity in the NP-B3 nanoparticles with 190 kDa HA coating was stronger compared with NP-B1 (possessing a 4.7 kDa HA coating) and NP-B2 (35 kDa HA coating) at the depth of 30 μm. This could be attributed to the fact that NP-B3 possess excellent mucus adsorption resistance and mucus permeation. These results confirmed that the HA coating on the NP-A core increased the efficiency of epithelial access of the NPs, especially when coating with HA of a high M_w. Moreover, to study the integrity of NP-A during the transport process, Cy5-insulin and FITC-CPP were co-localized in mucus layer at the bottom (30 μm in depth), as indicated by the overlap of green and red signals (yellow spots). It revealed that the NP-A cores were intact when arrived at the apical side of epithelium.

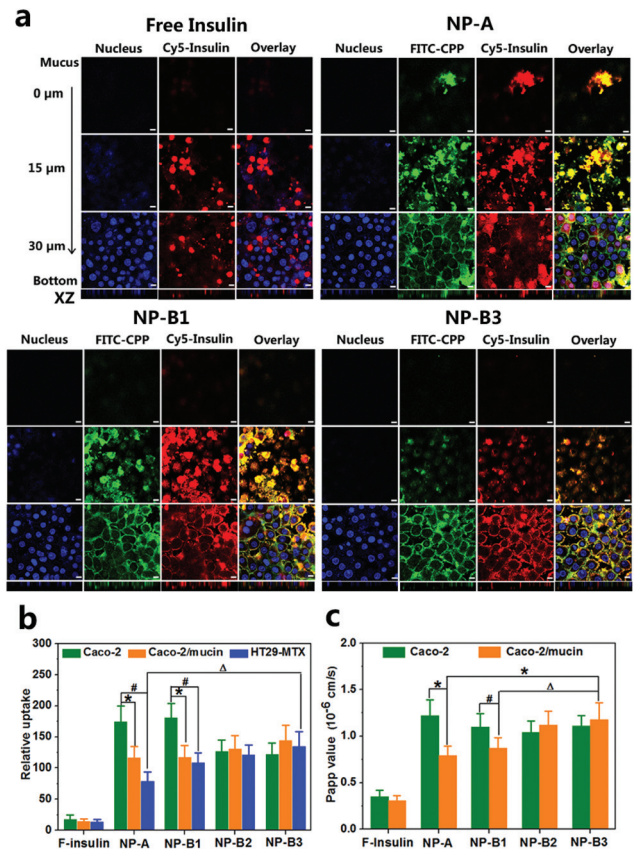

Fig. 3 Trans-epithelial transport property of NP-A and NP-B nanoparticles. (a) Nanoparticle-mediated insulin transport across mucus layer covered on HT29-MTX cell monolayer visualized by confocal microscopy imaging. NP-A, NP-B1 and NP-B3 were prepared from Cy5-labeled insulin and FITC-labeled CPP and incubated with HT29-MTX monolayer for 3 h before imaging. Free Cy-5 labeled insulin was applied as a control. Cell nuclei were stained with DAPI (shown in blue). Note: NP-A group (CPP/insulin); NP-B1 group (HA coating: 4.7 kDa); NP-B3 group (HA coating: 190 kDa). Scale bars: 10 μm. (b) Relative amounts of internalized NPs in Caco-2 or HT29-MTX cells; the relative amount of uptake was normalized by cell account (values are quantified by using the fluorescent intensity per 5.0×10^3 cells); $^{\#}p < 0.001$, $^{*}p < 0.001$, $^{\Delta}p < 0.01$. Data are shown as means ± SD ($n = 5$). (c) P_{app} values of tested samples across the Caco-2 monolayer in the trans-epithelial transport study; $^{*}p < 0.001$, $^{\Delta}p < 0.01$, $^{\#}p < 0.05$. Data are shown as means ± SD ($n = 4$).

Cellular internalization study

Caco-2 cell line is one of the most widely used cell lines for mimicking absorptive epithelial barrier in the small intestine. However, one limitation of Caco-2 monolayers is that it does not have mucus secreting function.[45] For this reason, we performed the uptake investigation using three different cultures: (1) Caco-2; (2) co-culture of Caco-2 with mucin (Caco-2/mucin (+)); and (3) mucus-secreting HT29-MTX cell line, to evaluate the epithelial uptake of the NP-A or NP-B and the influence of mucus on the uptake behavior. The results are shown in Fig. 3b. The cellular internalization of insulin was significantly better using NP-A or NP-B compared with free insulin solution in both cell models. Among NP-A and NP-B1/2/3, NP-B3 exhibited the highest uptake in HT29-MTX cell model, which was 11-fold higher than free insulin group and 1.9 times of that of NP-A. This indicated that the internalization performance on HT29-MTX cells can be improved by coating HA of a high M_w. Interestingly, the results in Caco-2 cell line were completely different from the results in HT29-MTX cell line. NP-B2 and NP-B3 exhibited a lower cellular uptake than the NP-A group, which might be attributed to the repulsion between the negatively-charged cell membrane of epithelia and the negatively-charged NP-B2-3. The good uptake efficiency of negatively charged NP-B1 on Caco-2 cell might be attributed to the assumption that the short-chain HA coating temporarily protects NP-A core and then undergoes detachment and exposes the positively-charged NP-A core to the apical surface of epithelium. In the co-culture of Caco-2 and mucin, a similar trend as HT29-MTX cell line was appreciated, *i.e.* NP-B samples had higher uptake than NP-A and NP-B3 was the best among NP-B1/2/3 nanoparticles, suggesting again that HA

Published on 25 January 2018. Downloaded by Columbia University Libraries on 4/28/2019 8:51:51 PM.

coating, especially that of a high M_w, help the NPs to survive the mucus layer.

Trans-epithelial transport study

The effect of NP-A/NP-B on promoting intestinal transcellular transportation was investigated in Caco-2 cell line, and Caco-2 cell line co-cultured with mucus, using a free-form insulin solution as a control. The apparent permeability coefficient (P_{app}) of insulin from the apical side to the basolateral side through the Caco-2 cell monolayer was monitored and results are shown in Fig. 3c. All tested insulin-loaded NP-A and NP-B exhibited higher P_{app} values compared with free insulin group. Positively charged NP-A exhibited highest trans-epithelial transport in Caco-2 cell model, and was 2.5-fold higher than that of free insulin group. Similar as the cellular internalization study, the presence of mucin has no significant effect on the transportation of NP-B2 and NP-B3; and NP-B3 exhibited the best transportation in mucin-containing cell model compared to mucin-free Caco-2 cell model. In contrast, the transportation of NP-A and NP-B1 were hampered significantly with the presence of mucin. Furthermore, it was observed that the trans-epithelial electrical resistance (TEER) values of the cell monolayers did not change over time when incubated with all tested NP-A or NP-B1/2/3 (Fig. S6†), indicating that the cell monolayer was intact and the transportation was mostly through transcellular pathway.

Distribution of dissociated HA shell in mucus layer

We had expected that the HA coated on the NP-B surface gradually detached from NP-A core during their permeation through the mucus layer, and this detachment played an important role for the downstream uptake or transcellular transportation. To further study the dissociation behavior of the HA shell on NP-B, the layered distribution of different components of NP-B on the HT29-MTX cell monolayer culture was observed using CLSM. As shown in Fig. 4, less Cy5-insulin (red) at the deeper depth of 30 μm and more entrapment of insulin at the depth of 15 μm were observed in NP-B1 comparing with NP-B3, which was consistent with the results of mucus permeation study. There were wide-spread scattered RITC-HA signals (green) without much co-localization with insulin (overlap of red and green, *i.e.* yellow) at the depth of 30 μm in NP-B1 group, while large portions of the Cy5-insulin (red) and RITC-HA (green) were co-localized at that depth, suggesting that the majority of NP-B3 were in their intact form before they reach the apical side of the epithelium. Notably, the widespread HA signals at the depth of 30 μm in all three NP-B groups might result from a fast diffusion of dissociated HA fragments in the mucus layer. Based on these observations, we proved that the 190 kDa HA coating on NP-B3 had the most suitable dissociation rate to achieve a slow dissociation in the mucus layer as well as the gradual exposure and deposition of the positively charged NP-A core to the epithelium. The dissociation of the 4.7 kDa HA coated on NP-B1 was too fast to protect NP-A core inside the mucus layer. The dissociation rate of the 35 kDa HA on NP-B2 was between NP-B1 and NP-B3 (Fig. S7 and S8†). The vertical distributions of HA (green) and insulin (red) in the mucus layer were observed under CLSM by using *Z*-axial scanning. The observation was consistent with the above results as well. In this study, the dissociation rate and location are optimized by varying the average molecular weight of the HA, assessed by CLSM imaging. Even though we do not know the exact mechanism by which HA detachment occurs, it is most likely due to the replacement of HA on nanoparticle surface by the negatively charged macromolecules in the extracellular milieu (*e.g.* proteins and glycoproteins) in the mucus layer with higher affinity with the positively charged nanoparticle core. The molecular weight of HA should influence the binding affinity and decomplexation tendency. By screening a wide range of molecular weights, we confirmed that the dissociation rate of the 190 kDa HA coating on NP-B3 was the most suitable in terms of a slow dissociation in the mucus layer and the gradual exposure and deposit of the positively charged NP-A core to the epithelium. It is worth noting that such a decomplexation process may result in new species on the nanoparticle surface, thus affecting cellular interaction and uptake of the nanoparticles.

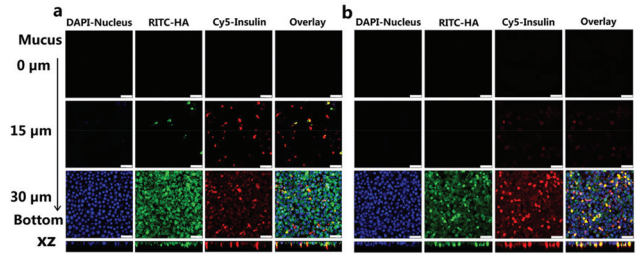

Fig. 4 CLSM images showing the distribution of HA and insulin in NP-B nanoparticles through the mucus layer of HT29-MTX cell monolayer from apical to bottom side. NP-B1 and NP-B3 were prepared from Cy5-labeled insulin and RITC-labeled HA and incubated with HT29-MTX monolayer for 2 h before imaging. Blue: DAPI-cell nuclei; green: RITC-HA; red: Cy5-Insulin; yellow: co-localization of Cy5-insulin and RITC-HA. Scale bars: 50 μm. CLSM images on *XZ* axis represent the vertical distribution of HA and insulin on mucus layer of HT29-MTX cell monolayer. (a) NP-B1 nanoparticles (HA coating: 4.7 kDa); (b) NP-B3 nanoparticles (HA coating: 190 kDa).

In vivo absorption of NPs

To further confirm the role of HA coating on nanoparticle transport through mucus layer and transport through epithelium, we orally fed the normal rats with NP-A and NP-B1/2/3 nanoparticles prepared with Cy3-labeled insulin, and harvested jejunum at 2 h after oral dosing, and examined the nanoparticle distribution throughout the mucus (visualized with Alexa Fluor 647-conjugated wheat germ agglutinin) and microvilli. For free insulin and NP-A groups, few Cy3-insulin signals (shown in red, Fig. 5) were detected in the villi, indicating poor absorption. Strong Cy3-insulin signals were observed in the mucus layer (shown in green, Fig. 5) for NP-A. In contrast to the NP-A group, appreciable absorption of Cy3-insulin was observed in the epithelial cells for all NP-B NPs. In particu-

 This journal is © The Royal Society of Chemistry 2018

Published on 25 January 2018. Downloaded by Columbia University Libraries on 4/28/2019 8:51:51 PM.

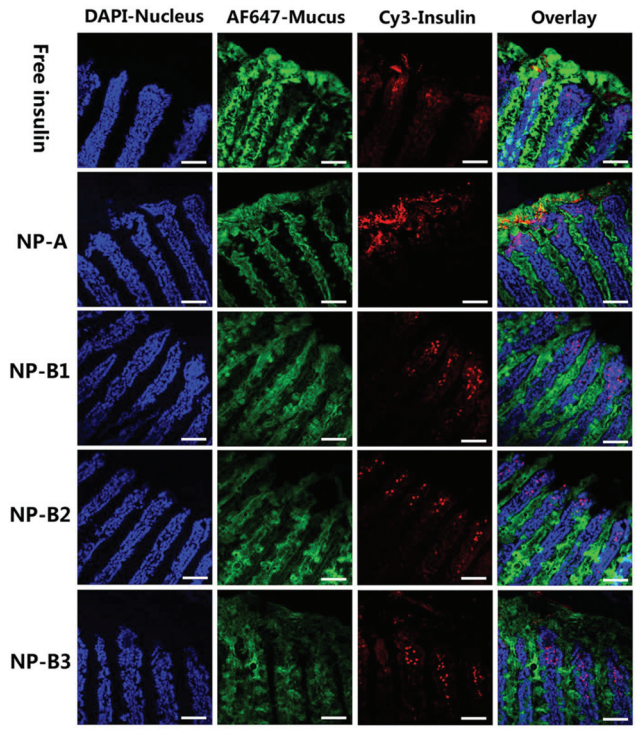

Fig. 5 Representative fluorescence images of rat intestinal villi (segment: jejunum) after oral administration of various nanoparticle formulations with Cy3-labeled insulin. Free insulin solution was included as a negative control in comparison with NP-A, NP-B1 (HA coating: 4.7 kDa), NP-B2 (HA coating: 35 kDa) and NP-B3 (HA coating: 190 kDa) nanoparticle formulations. Tissue sections were stained with WGA-647 (green) and DAPI (blue) to visualize the mucus and nucleus. Scale bars: 50 μm.

lar, NP-B3 exhibited the strongest signal within the villi among all NP-B1/2/3 groups; and most of the signals were observed in the interior of villi, where the villus capillaries are located. This result was consistent with the *in vitro* mucin affinity study and mucus permeation study, suggesting that higher retention in mucus layer may occur for NP-A, but much less for NP-B. This result also demonstrated again that the NP-B3 nanoparticles, which has a 190 kDa HA coating, were the most effective in shepherding NP-A nanoparticles through the mucus layer and delivering insulin to the villus capillaries.

Pharmacological and pharmacokinetics analysis

We evaluated the glucose reduction effect and pharmacokinetics of insulin following oral administration of the NP-A or NP-B on a Type I diabetes rat model established as reported in the literature.[9,16] In a pilot study, we tested p.o. administration of insulin loaded NPs at both 50 and 80 IU kg^{-1} doses. A dose of 80 IU kg^{-1} (NP-B) of insulin generated a significantly high level of glucose reduction (NP-B3: 60%) in a sustained manner, whereas p.o. administration at a dose of 50 IU kg^{-1} yielded a much lower level (~40%) of reduction in blood glucose concentration (Fig. S9a†). Based on these results, we chose the dose of 80 IU kg^{-1} for the pharmacological and pharmacokinetics studies. The negative control group was administered with deionized water. The pharmacodynamic profiles of all tested groups are shown in Fig. 6a. In the positive control group that received a subcutaneous (s.c.) injection of free insulin solution (5 IU kg^{-1}), the blood glucose level was reduced sharply to about 25% of the basal level within 1 h and remained at that level for about 4 h. Similar to the deionized water-fed group, oral administration of free-form insulin solution failed to reduce the blood glucose level. The administration of NP-B3 solution (80 IU kg^{-1}) generated a drastic level of glucose reduction by 60% in a sustained manner. There was no distinct difference among NP-A, NP-B1 and NP-B2 on blood glucose reduction during the first 5 h, while NP-B2 exhibited a significant and durable glucose reduction effect later (5–8 h post oral administration). The hypoglycemic profiles with absolute blood glucose level are shown in Fig. S9a.† The pharmacological availabilities (PA%) of NC, NP-B1, NP-B2, and NP-B3 were 2.6%, 2.8%, 3.0% and 3.7%, respectively. These results demonstrated the effectiveness of our insulin-loaded NP-B3 on reducing blood glucose levels of diabetic rats gradually following the oral dosing. In comparison, NP-A and NP-B1 elicited milder response.

To evaluate the protective effect of enteric coating against the harsh acid environment in stomach, we then tested the glucose reduction effect of MCs following oral administration using the same animal model. As shown in Fig. 6b, the glucose reduction effects of NP-B2 and NP-B3-loaded MCs (MC-2/3) were better than NP-B1-loaded MCs (MC-1), and induced gradual but marked reduction of blood glucose levels by 63% (for MC-2) and 80% (MC-3) in contrast to 53% for MC-1. On the other hand, the uncoated NP-B2 and NP-B3 nanoparticles yielded milder reduction of blood glucose levels, by 55% and 62%, respectively, within 8 h at a same dose of 80 IU kg^{-1}. The hypoglycemic profiles with absolute blood glucose level are shown in Fig. S9b.† These results demonstrated that the acid resistance and pharmaco-dynamics performance of NP-B nanoparticles were significantly improved after enteric coating. The pharmacokinetic profiles of insulin-loaded nanoparticles were shown in Fig. 6c. Orally administered MC-2 and MC-3 generated a slow rise in serum insulin concentration, which reached their corresponding maximal concentrations at 4 h. As a control, s.c. injection of free-form insulin solution at 5 IU kg^{-1} resulted in a rapid increase in serum insulin concentration. The relative bioavailability of MC-3 was estimated to be 11%, which is significantly higher than that of MC-1 (5.3%) and MC-2 (7.4%). Given what we observed in the above *in vitro* and *in vivo* experiments, the superior performance of MC-3 could be attributed to the most effective coating by HA with the highest M_w. Although the bioavailability of MC-3 is similar to another system we reported previously using large enteric capsules,[2] the scalable encapsulation of NP-B nanoparticles into MCs using this continuous production process is distinctively advantageous. Besides the ease of production, the MCs are likely to improve the consistency and reliability of the delivery outcomes due to the more widespread distribution of MCs in GI track with a single dose

Published on 25 January 2018. Downloaded by Columbia University Libraries on 4/28/2019 8:51:51 PM.

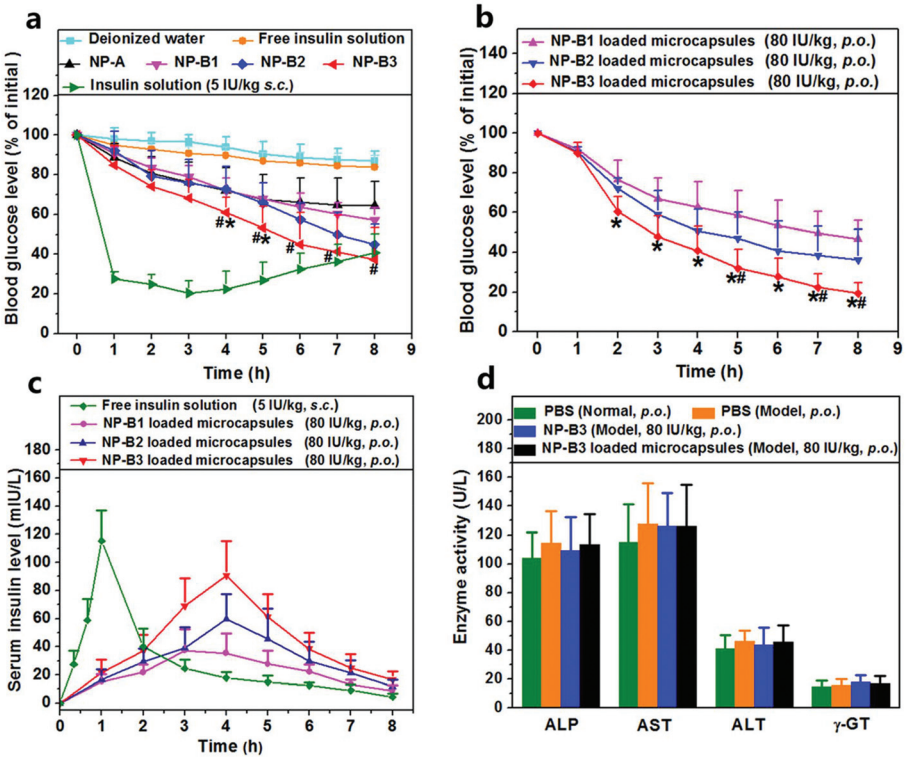

Fig. 6 Efficacy of insulin-loaded nanoparticles. (a) Variation of blood glucose levels of fasting diabetic rats following oral administration of deionized water (as a background control), free insulin (as a negative control) and different insulin formulations (insulin dose: 80 IU kg^{-1}), or following subcutaneous (s.c.) injection free insulin solution at dose of 5 IU kg^{-1} (as a positive control). $^{\#}p < 0.05$ for NP-B3 *vs.* NP-B1 group; $*p < 0.05$ for NP-B3 *vs.* NP-B2 group. Data are shown as means ± SD (n = 8). (b) Variation of blood glucose levels of diabetic rats after orally administering MC-1/2/3 (*i.e.* HPMCP-coated NP-B1/2/3 nanoparticles) at an insulin dose of 80 IU kg^{-1}, $*p < 0.05$ *vs.* NP-B1 loaded MC group; $^{\#}p < 0.05$ *vs.* NP-B2 loaded MC group. Data are shown as means ± SD (n = 6). (c) Variation of serum insulin level of diabetic rats after orally administering MC-1/2/3 particles at dose of 80 IU kg^{-1}, or s.c. injection with insulin solution at 5 IU insulin per kg. Data are shown as means ± SD (n = 6). (d) Serum levels of alkaline phosphatase (ALP), alanine transaminase (ALT), aspartate transaminase (AST) and γ-glutamyl transpeptidase (γ-GT) in diabetic rats after 7 days of consecutive oral administration of PBS, MC-1 and MC-3 suspension. Normal rats receiving PBS solution were used as a control group. Data are shown as mean ± SD (n = 6).

in comparison with a single large enteric capsule. The pH-induced dissolution process is also likely to be more rapid than a large capsule. These features could add more appeal to these MCs produced by this sequential FNC process.

In conclusion, NP-B-loaded MCs could generate an excellent glucose reduction response, reaching the normal blood glucose level (~5 mM) within 8 h after oral dosing. In addition, liver function analysis (Fig. 6d) and histomorphology observation (Fig. S10†) confirmed the biocompatible nature of these NPs and MCs. These data further support that the NP-B-loaded MCs are a promising candidate for oral delivery of insulin.

Conclusions

In this study, we devised a strategy to fabricate multifunctional protein nanoparticles for oral administration therapy through a sequential FNC procedure. Using this system, the protein-encapsulating nanoparticles with improved properties of acid-stability in stomach, high permeation on mucus layer, and sufficient trans-epithelia transport was obtained *via* a step-by-step FNC process. With detailed *in vitro* and *in vivo* characterization, the NP-A core coated with higher M_W HA demonstrated the best performance to overcome both the mucus barrier and epithelial barrier, and control the blood sugar level effectively. The enteric coating added to the NP-B nanoparticles proved effective as a convenient modification to ensure effective protection in the gastric cavity and timely release of nanoparticles in the intestinal track. The effective oral delivery of small proteins such as insulin using this system raises great prospect that this delivery system and nanoparticle fabrication strategy could be applicable to many other protein therapeutics and gene medicine candidates. In addition, this study expands the capability of flash nanocomplexation and flash nanoprecipitation as a continuous nanoparticle manufacture method to coating and encapsulation of nanoparticles, thus allowing incorporating additional functionalities in a scalable fashion with ease.

Conflicts of interest

There are no conflicts to declare.

 This journal is © The Royal Society of Chemistry 2018

Published on 25 January 2018. Downloaded by Columbia University Libraries on 4/28/2019 8:51:51 PM.

Acknowledgements

This work was supported by the Guangdong Innovative and Entrepreneurial Research Team Program (No. 2013S086), Natural Science Foundation of Guangdong Province (No. 2014A030312018), and Natural Science Foundation of China (No. 51533009).

References

1 J. L. Santos, Y. Ren, J. Vandermark, M. M. Archang, J. M. Williford, H. W. Liu, J. Lee, T. H. Wang and H. Q. Mao, *Small*, 2016, **12**, 6214–6222.
2 Z. He, J. L. Santos, H. Tian, H. Huang, Y. Hu, L. Liu, K. W. Leong, Y. Chen and H. Q. Mao, *Biomaterials*, 2017, **130**, 28–41.
3 S. Satake, M. C. Moore, K. Igawa, M. Converse, B. Farmer, D. W. Neal and A. D. Cherrington, *Diabetes*, 2002, **51**, 1663–1671.
4 W. B. Geho, H. C. Geho, J. R. Lau and T. J. Gana, *J. Diabetes Sci. Technol.*, 2009, **3**, 1451–1459.
5 R. L. Chin, R. Martinez and G. Garmel, *Am. J. Emerg. Med.*, 1993, **11**, 622–625.
6 S. Soares, A. Costa and B. Sarmento, *Expert Opin. Drug Delivery*, 2012, **9**, 1539–1558.
7 L. M. Ensign, R. Cone and J. Hanes, *Adv. Drug Delivery Rev.*, 2012, **64**, 557–570.
8 M. C. Chen, K. Sonaje, K. J. Chen and H. W. Sung, *Biomaterials*, 2011, **32**, 9826–9838.
9 W. Shan, X. Zhu, M. Liu, L. Li, J. Zhong, W. Sun, Z. Zhang and Y. Huang, *ACS Nano*, 2015, **9**, 2345–2356.
10 S. Correa, K. Y. Choi, E. C. Dreaden, K. Renggli, A. Shi, L. Gu, K. E. Shopsowitz, M. A. Quadir, E. Ben-Akiva and P. T. Hammond, *Adv. Funct. Mater.*, 2016, **26**, 991–1003.
11 Q. Xu, L. M. Ensign, N. J. Boylan, A. Schoen, X. Gong, J.-C. Yang, N. W. Lamb, S. Cai, T. Yu, E. Freire and J. Hanes, *ACS Nano*, 2015, **9**, 9217–9227.
12 R. A. Cone, *Adv. Drug Delivery Rev.*, 2009, **61**, 75–85.
13 K. W. Smithson, D. B. Millar, L. R. Jacobs and G. M. Gray, *Science*, 1981, **214**, 1241–1244.
14 J. D. Ramsey and N. H. Flynn, *Pharmacol. Ther.*, 2015, **154**, 78–86.
15 E. J. Nielsen, S. Yoshida, N. Kamei, R. Iwamae, S. Khafagy el, J. Olsen, U. L. Rahbek, B. L. Pedersen, K. Takayama and M. Takeda-Morishita, *J. Controlled Release*, 2014, **189**, 19–24.
16 X. Zhu, J. Wu, W. Shan, Z. Zhou, M. Liu and Y. Huang, *Adv. Funct. Mater.*, 2016, **26**, 2728–2738.
17 J. Sheng, H. He, L. Han, J. Qin, S. Chen, G. Ru, R. Li, P. Yang, J. Wang and V. C. Yang, *J. Controlled Release*, 2016, **233**, 181–190.
18 E. J. B. Nielsen, N. Kamei and M. Takeda-Morishita, *Biol. Pharm. Bull.*, 2015, **38**, 144–146.
19 S. Khafagy el, R. Iwamae, N. Kamei and M. Takeda-Morishita, *AAPS J.*, 2015, **17**, 1427–1437.
20 N. Kamei, M. Morishita, Y. Eda, N. Ida, R. Nishio and K. Takayama, *J. Controlled Release*, 2008, **132**, 21–25.
21 H. Y. Yoon, H. Koo, K. Y. Choi, S. J. Lee, K. Kim, I. C. Kwon, J. F. Leary, K. Park, S. H. Yuk, J. H. Park and K. Choi, *Biomaterials*, 2012, **33**, 3980–3989.
22 H. Y. Yoon, H. Koo, K. Y. Choi, I. Chan Kwon, K. Choi, J. H. Park and K. Kim, *Biomaterials*, 2013, **34**, 5273–5280.
23 C. M. Hsieh, Y. W. Huang, M. T. Sheu and H. O. Ho, *Int. J. Biol. Macromol.*, 2014, **64**, 45–52.
24 H.-W. Sung, K. Sonaje, Z.-X. Liao, L.-W. Hsu and E.-Y. Chuang, *Acc. Chem. Res.*, 2012, **45**, 619–629.
25 Z. M. Wu, L. Zhou, X. D. Guo, W. Jiang, L. Ling, Y. Qian, K. Q. Luo and L. J. Zhang, *Int. J. Pharm.*, 2012, **425**, 1–8.
26 E. A. Hosny, H. I. Al-Shora and M. M. A. Elmazar, *Int. J. Pharm.*, 2002, **237**, 71–76.
27 A. M. Sadeghi, F. A. Dorkoosh, M. R. Avadi, P. Saadat, M. Rafiee-Tehrani and H. E. Junginger, *Int. J. Pharm.*, 2008, **355**, 299–306.
28 M. Lopes, N. Shrestha, A. Correia, M. A. Shahbazi, B. Sarmento, J. Hirvonen, F. Veiga, R. Seica, A. Ribeiro and H. A. Santos, *J. Controlled Release*, 2016, **232**, 29–41.
29 Z. Liu and P. Yao, *Polym. Chem.*, 2014, **5**, 1072–1081.
30 X. Y. Yang, Y. X. Li, M. Li, L. Zhang, L. X. Feng and N. Zhang, *Cancer Lett.*, 2013, **334**, 338–345.
31 H. Tian, L. Lin, J. Chen, X. Chen, T. G. Park and A. Maruyama, *J. Controlled Release*, 2011, **155**, 47–53.
32 T. Jiang, Z. Zhang, Y. Zhang, H. Lv, J. Zhou, C. Li, L. Hou and Q. Zhang, *Biomaterials*, 2012, **33**, 9246–9258.
33 K. Sonaje, Y.-J. Chen, H.-L. Chen, S.-P. Wey, J.-H. Juang, H.-N. Nguyen, C.-W. Hsu, K.-J. Lin and H.-W. Sung, *Biomaterials*, 2010, **31**, 3384–3394.
34 N. Sawtarie, Y. Cai and Y. Lapitsky, *Colloids Surf., B*, 2017, **157**, 110–117.
35 Y. H. Lin, K. Sonaje, K. M. Lin, J. H. Juang, F. L. Mi, H. W. Yang and H. W. Sung, *J. Controlled Release*, 2008, **132**, 141–149.
36 M. R. Rekha and C. P. Sharma, *J. Controlled Release*, 2009, **135**, 144–151.
37 A. Makhlof, Y. Tozuka and H. Takeuchi, *Eur. J. Pharm. Sci.*, 2011, **42**, 445–451.
38 Z. Zhu, *Mol. Pharm.*, 2014, **11**, 776–786.
39 S. F. Chow, C. C. Sun and A. H. Chow, *Eur. J. Pharm. Biopharm.*, 2014, **88**, 462–471.
40 S. Jeon, C. Y. Yoo and S. N. Park, *Colloids Surf., B*, 2015, **129**, 7–14.
41 J. Hernandez-Montelongo, V. F. Nascimento, D. Murillo, T. B. Taketa, P. Sahoo, A. A. de Souza, M. M. Beppu and M. A. Cotta, *Carbohydr. Polym.*, 2016, **136**, 1–11.
42 K. Margulis, S. Magdassi, H. S. Lee and C. W. Macosko, *J. Colloid Interface Sci.*, 2014, **434**, 65–70.
43 S. M. D'Addio and R. K. Prud'homme, *Adv. Drug Delivery Rev.*, 2011, **63**, 417–426.
44 A. A. Date, J. Hanes and L. M. Ensign, *J. Controlled Release*, 2016, **240**, 504–526.
45 N. Reix, A. Parat, E. Seyfritz, R. Van der Werf, V. Epure, N. Ebel, L. Danicher, E. Marchioni, N. Jeandidier, M. Pinget, Y. Frere and S. Sigrist, *Int. J. Pharm.*, 2012, **437**, 213–220.